OPEN ACCESS Freely available online

PLOS ONE

Characterization and Modeling Analysis for Metal-Semiconductor-Metal GaAs Diodes with Pd/SiO_2 Mixture Electrode

Shih-Wei Tan*, Shih-Wen Lai

Department of Electrical Engineering, National Taiwan Ocean University, Keelung, Taiwan, Republic of China

Abstract

Characterization and modeling of metal-semiconductor-metal (MSM) GaAs diodes using to evaporate SiO_2 and Pd simultaneously as a mixture electrode (called M-MSM diodes) compared with similar to evaporate Pd as the electrode (called Pd-MSM diodes) were reported. The barrier height (ϕ_b) and the Richardson constant (A*) were carried out for the thermionic-emission process to describe well the current transport for Pd-MSM diodes in the consideration of the carrier over the metal-semiconductor barrier. In addition, in the consideration of the carrier over both the metal-semiconductor barrier and the insulator-semiconductor barrier simultaneously, thus the thermionic-emission process can be used to describe well the current transport for M-MSM diodes. Furthermore, in the higher applied voltage, the carrier recombination will be taken into discussion. Besides, a composite-current (CC) model is developed to evidence the concepts. Our calculated results are in good agreement with the experimental ones.

Citation: Tan S-W, Lai S-W (2012) Characterization and Modeling Analysis for Metal-Semiconductor-Metal GaAs Diodes with Pd/SiO_2 Mixture Electrode. PLoS ONE 7(11): e50681. doi:10.1371/journal.pone.0050681

Editor: Jeongmin Hong, Florida International University, United States of America

Received September 12, 2012; **Accepted** October 26, 2012; **Published** November 30, 2012

Funding: This work is financially supported by the National Taiwan Ocean University of the Republic of China under the contract No. NTOU-100-014 and 101B290031. The funders had no role in study design, data collection and analysis, decision to publish, or preparation of the manuscript.

Competing Interests: The authors have declared that no competing interests exist.

* E-mail: tanshwei@mail.ntou.edu.tw

Introduction

The metal-semiconductor (MS) contact and the metal-oxide-semiconductor (MOS) capacitor are the most useful device in the study of semiconductor surfaces and essential component in semiconductor device. MS contact with rectifying characteristic is widely used in MESFETs, HEMTs, optical sensors, and gas sensors. MOS capacitor with voltage-controlled variable is used in MOSFETs for forefront high-density integrated circuits [1–4]. Recently, Hydrogen has been widely used in hydrogen-fueled vehicles, medical treatment, chemical industry, and semiconductor fabrication. However, hydrogen-containing gases have the risk to cause explosion. Therefore, the development of hydrogen sensors for real-time in situ detection is highly required. A number of palladium and platinum-based hydrogen sensors have been demonstrated [5–22]. Among them, MS diodes [5–13] have been addressed to be one of the most promising devices. Hydrogen sensors employing MOS diodes have also been extensively studied [14–18].

In addition, Chiu et al. [19–22] reported a new MSM hydrogen sensor with two multifinger Schottky contacts. Unlike conventional MS and MOS diodes, a mixture of palladium and silicon dioxide (SiO_2) is deposited upon the semiconductor layer. Compared to commonly used MS and MOS diodes, M-MSM diodes obtained excellent performance of high sensitivity. However, the current–voltage (I–V) curve represents the diode current operated as sensor in N_2. I-V curve for M-MSM diodes differ from one for MS diodes in that the former exhibit the multiple-step phenomenon, while the latter are not. The reason of causing the multiple-step phenomenon is very interesting but there are no descriptions in Chiu et al. reported [22]. In this paper, characterization and modeling of M-MSM GaAs diodes were reported. The ϕ_b and the A* were determined by a deduced equations from the I-V curve that operated at various temperature. The carrier over both the metal-semiconductor barrier and the insulator-semiconductor barrier are considered simultaneously on the thermionic emission process that can be used to describe well the current transport for M-MSM diodes. With increasing the applied voltage, the number of minority carrier at the semiconductor surface is larger than of the majority carrier. The carrier recombination will be taken into consideration. Furthermore, a composite current (CC) model is developed to evidence the concepts. The calculated results are in good agreement with the experimental ones. Finally, conclusions were made.

Device Structure and Fabrication

The epitaxial structure was grown on a (100)-oriented GaAs substrate by LP-MOCVD. It consisted of a 0.6 μm n^+-GaAs layer, and a 0.8 μm n-GaAs layer with 8×10^{16} cm^{-3} doping concentration. The process started with mesa isolation. HCl was used to remove the native oxide on the 0.8 μm n-GaAs layer after a device mesa. Two multiple-fingers Schottky electrodes forming a MSM diodes were implemented by thermally depositing a 30 nm mixture with various weight-ratios of Pd to SiO_2. Both the finger width and the finger-to-finger spacing are 5 μm. The area of the multiple-fingers electrode was $A \approx 8\times10^{-4}$ cm^2. Another MSM diodes with a 30 nm Pd directly deposited upon the GaAs layer was also fabricated for comparison. Device measurement was

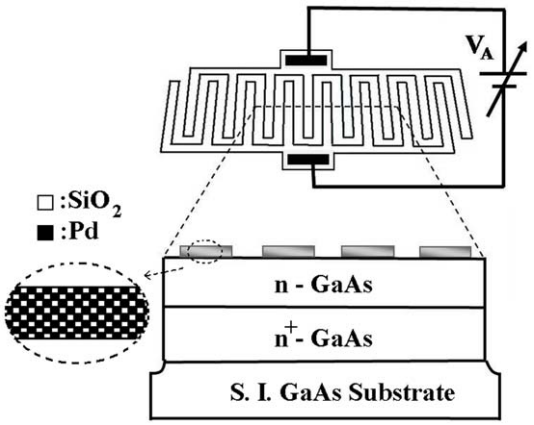

Figure 1. Schematic view of a M-MSM diodes with two multi-finger Pd/SiO_2 mixture electrodes.
doi:10.1371/journal.pone.0050681.g001

carried out by a custom-made 235 ml flow-through test chamber made from stainless steel and filled with the 99.99% nitrogen gas at a flow rate of 500 sccm. Fig. 1 shows the schematic views for the finally fabricated M-MSM diodes.

Determination of Barrier Height and Richardson Constant

I–V curves of Pd-MSM diodes at various temperatures in the range of 300 K to 330 K are shown in Fig. 2. The solid symbols are the calculated results. Because the quality of the epitaxial wafer and the evaporative Pd are excellent and uniform, all curves indicate bidirectional and symmetrical. The thermionic-emission process for carrier and the image-force lowering are considered simultaneously on the current of Pd-MSM diodes (I_{Pd}), I_{Pd} can be expressed as [23].

$$I_{Pd} = A^{*}\cdot A\cdot T^{2}\cdot e^{-\frac{q\left\{\phi_b-\left[\frac{q^3N_d}{8\pi^2\varepsilon_o{}^3(\varepsilon_S')^2\varepsilon_S}\left(\phi_b-V_n-\frac{kT}{q}-V\right)\right]^{0.25}\right\}}{kT}} \quad (1)$$

where $A^* = 8.9$ A/k-cm^2 is the Richardson constant for GaAs and be given by

$$A^{*} = \exp\left(\frac{T_2\cdot\ln\left(\frac{I_2}{A\cdot T_2^2}\right)-T_1\cdot\ln\left(\frac{I_1}{A\cdot T_1^2}\right)}{T_2-T_1}\right), \quad (2)$$

and $\phi_b = 0.80$ eV is the barrier height and be given by

$$\phi_b = -\frac{k\cdot\ln\left(\frac{I_1\cdot T_2^2}{I_2\cdot T_1^2}\right)}{q\cdot\left(\frac{1}{T_1}-\frac{1}{T_2}\right)} \quad (3)$$

Other parameters of A ≈ 8×10−4 cm2, T = 300 K to 330 K, q = 1.6×10−19 C [23], k = 1.38×10−23 J/K [23], N_d = 8×1016 cm−3, ε_o = 8.85×10−14 F/cm [23], ε_S' = 10.8, ε_S = 12.9 [23], Vn = 0.05 V, V = 0 V to 5V are the contact area, an absolute temperature, the unit electronic charge, the Boltzmann constant, the doping concentration, the permittivity of free space, the relative permittivity of GaAs near the Pd, the relative permittivity of GaAs, the Fermi potential from conduction-band edge, and an applied voltage, respectively. Following the previous article [24], the electron approaches the metal with the thermal velocity, and one might except that there is not enough time for the semiconductor to become fully polarized by the electric field, so that ε_S' is less then ε_S. For our calculation in Fig. 2, the results are also represented with a good agreement found. This means that the I_{Pd} together with the extracted device-parameters is very promising for well describing for Pd MSM diodes behaviors.

Experimental Performance and Modeling Deducing

Unlike the Fig. 2 represented I_{Pd}, Fig. 3 shows I–V curves with a multiple-step phenomenon of M-MSM diodes with the mixture electrodes in the weight-ratio of SiO_2 to Pd equal to 1/3 at various temperatures in the range of 300 K to 330 K. The solid symbols are the calculated results. In order to probe into the multiple-step phenomenon in I–V curves, Fig. 4(a) shows the ϕ_b as a function of the applied voltage for M-MSM diodes with the mixture electrodes in the weight-ratio of SiO_2 to Pd equal to 1/3, ϕ_b as function of applied voltage for Pd-MSM diodes is also included for comparison. The line slope, $-\frac{\partial\phi_b}{\partial V}$, shows the multiple-step phenomenon and indicates that the carrier over both the

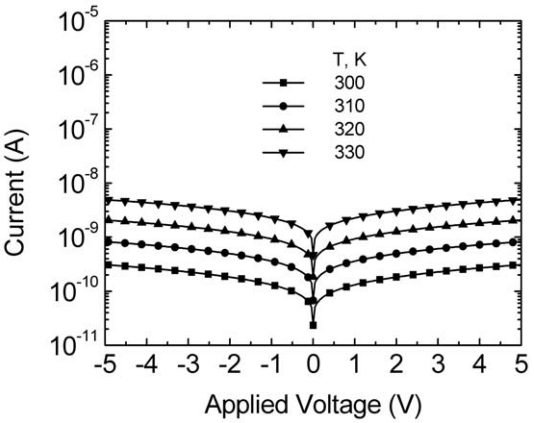

Figure 2. Currents as a function of applied voltage for Pd-MSM diodes at various temperatures. Calculated data are included.
doi:10.1371/journal.pone.0050681.g002

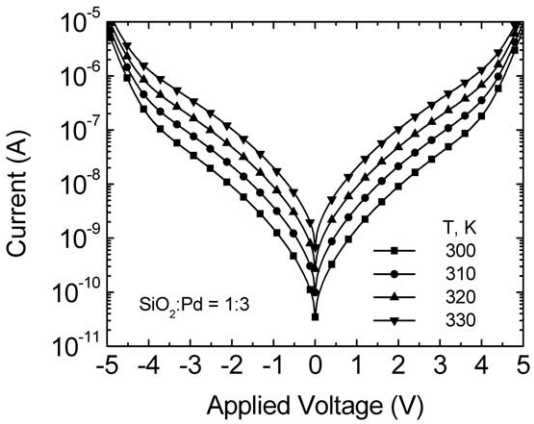

Figure 3. Currents as a function of applied voltage for M-MSM diodes with weight-ratio of SiO_2 and Pd equal to 1:3 in mixture at various temperatures. Calculated data are included.
doi:10.1371/journal.pone.0050681.g003

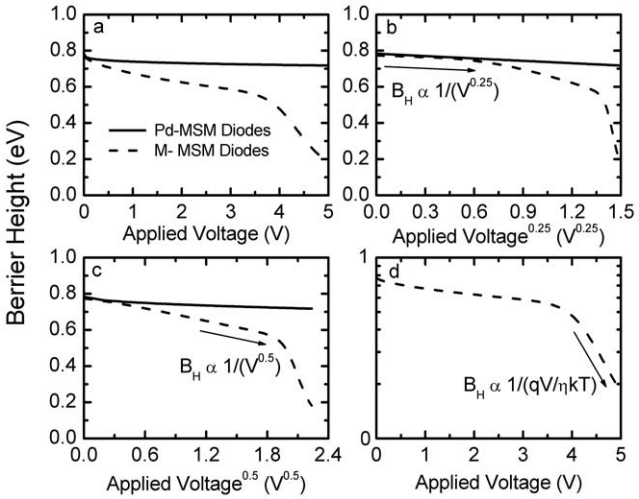

Figure 4. Barrier height (ϕ_b) as a function of (a) applied voltage, (b) applied voltage to the power of 0.25, (c) applied voltage to the power of 0.5, and (d) lnϕ_b as a function of applied voltage for a Pd-MSM diodes (solid lines) and a M-MSM diodes (dashed lines).
doi:10.1371/journal.pone.0050681.g004

metal-semiconductor barrier and the insulator-semiconductor barrier together with image-force lowering are considered on the thermionic emission process. That is, to notice Fig. 4 (b), ϕ_b against $V^{0.25}$ represents a straight line from $V^{0.25} = 0$ V to 0.58 V. Hence, the current component of the thermionic-emission process for carrier over the metal-semiconductor barrier (I_{MS}) is considered on the CC model for M-MSM diodes (I_M), I_{MS} can be expressed as

$$I_{MS} = A^* \cdot A_{Pd} \cdot T^2 \cdot e^{-\frac{q\left\{\phi_B - \left[\frac{q^3 N_d}{8\pi^2 \varepsilon_o^3 (\varepsilon_S')^2 \varepsilon_S}\left(\phi_B - V_n - \frac{kT}{q} - V\right)\right]^{0.25}\right\}}{kT}} \quad (4)$$

where $A^* = 9.6$ A/k-cm^2 and $\phi_B = 0.81$ eV are given by Eq.2 and Eq.3, respectively. $A_{Pd} \approx 2.90 \times 10^{-4}$ cm^2 and $\varepsilon_S' = 7.01$ are the effective Pd-contact area and the relative permittivity of GaAs near the mixture, respectively. Other parameters are the same as previous. Similarly, to notice Fig. 4 (c), ϕ_b against $V^{0.5}$ represents a straight line from $V^{0.5} = 1.2$ V to 1.9 V. For that reason, the current component of thermionic-emission process for carrier over the insulator-semiconductor barrier (I_{MIS}) is considered on I_M, I_{MIS} can be expressed as [23]

$$I_{MIS} = A^* \cdot A_{ox} \cdot T^2 \cdot e^{-\frac{q\left\{\phi_B - \sqrt{\frac{qV}{4\pi\varepsilon_o \varepsilon_i d}}\right\}}{kT}} \quad (5)$$

where the effective oxide-contact area is $A_{ox} \approx 5.10 \times 10-4$ cm2. The $\varepsilon_i = 3.56$ [23] and the d = 30 nm are the relative permittivity and the thickness of mixture, respectively. Other parameters are the same as IMS. To notice Fig. 4 (d), lnϕ_b against V represents a straight line with the applied voltage larger then 4 V. When a larger voltage is applied (>4 V), the bands bend even more downward so that the intrinsic level Ei at the surface crosses over the Fermi level EF. At this point the number of holes (minority carriers) at the surface is larger then that of the electrons, the thermionic-emission of electrons will be recombined by holes and the current is proportional to qV/ηkT. Therefore, the current

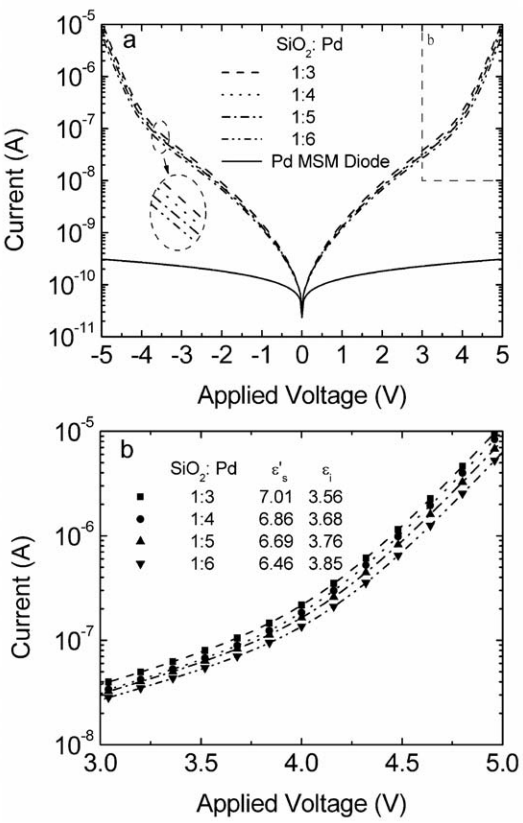

Figure 5. Currents as a function of applied voltage for M-MSM diodes with various weight-ratios of SiO_2 and Pd at 300 K. Calculated data are included.
doi:10.1371/journal.pone.0050681.g005

component of recombination (IRB) is considered on IM. The current IRB can be expressed as [23]

$$I_{RB} = I_{RBS} \cdot e^{\frac{qV}{\eta kT}} \quad (6)$$

where IRBS = 4.81×10−16 A, and η = 8.1 are the saturation current of recombination, and an ideality factor, respectively. Then, IM can be approximated by the sum of Eqs. 4, Eqs. 5, and Eqs. 6. In Fig. 3, calculated results at various temperatures are also included with a good agreement found. This means that IM together with the extracted parameters is very promising for well describing M-MSM diodes behaviors.

Figure 5(a) shows I–V characteristics of M-MSM diodes with the mixture electrodes in various weight-ratios of SiO_2 to Pd. I–V characteristic of Pd-MSM diodes is also shown for comparison. I_M that were marked by solid symbol together with the extracted parameters are shown in Fig. 5(b). I_M together with the extracted parameters is very promising for well describing the experimental results.

On the other hand, ε_s' and ε_i associated with the mixture in various weight-ratios of SiO_2 to Pd are the key parameters and play an important role on the performance of M-MSM diodes. For simplifying the calculation of the relative permittivity, the composition of mixture is uniform for assumption. Fig. 6 shows the schematic view of Pd/SiO_2 mixture electrode for M-MSM diodes. ε_s' is proportional to the ratio of A_{Pd} and A_{ox}, So the effective relative permittivity of GaAs near the mixture ($\varepsilon_{s,eff}'$) can be calculated as

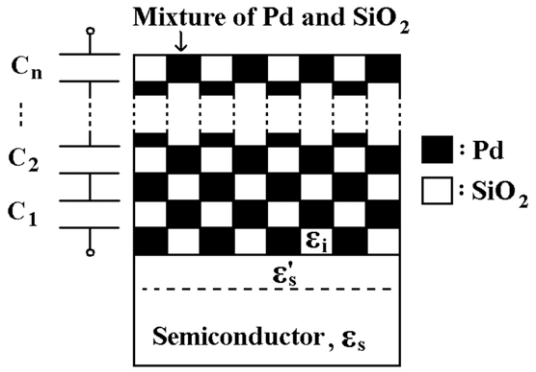

Figure 6. Schematic view of Pd/SiO_2 mixture electrode for M-MSM diodes to calculate the effective relative permittivity.
doi:10.1371/journal.pone.0050681.g006

$$\varepsilon'_{s,eff} = \frac{10.8 \cdot A_{Pd} + 3.9 \cdot A_{ox}}{A_{Pd} + A_{ox}} \quad (7)$$

Consideration of equivalent circuit, the capacitance of mixture can be expressed as

$$C_M = \frac{1}{C_1} + \frac{1}{C_2} + \ldots + \frac{1}{C_n} = \frac{1}{C_{ox}} + \frac{1}{C_{ox}} + \ldots + \frac{1}{C_{ox}} = \frac{n}{C_{ox}} = \varepsilon_{i,eff} \cdot \frac{A}{d},$$

where $C_{ox} = \varepsilon_i \cdot \frac{(L_{ox} + L_{Pd}) \cdot n}{L_{ox} \cdot d} \cdot A \cdot \frac{A_{ox}}{A_{ox} + A_{Pd}}$ is the capacitance of SiO_2, L_{pd}, L_{ox}, A, and d are the Pd thickness, the SiO_2 thickness for mixture, the contact area, the thickness of mixture, respectively. Then the effective relative permittivity of mixture ($\varepsilon_{i,eff}$) can be deduced to

$$\varepsilon_{i,eff} = \frac{3.9}{\frac{L_{Pd} + L_{ox}}{L_{ox}} \cdot \frac{A_{ox}}{A_{pd} + A_{ox}}} \quad (8)$$

$\varepsilon'_{s,eff}$ and $\varepsilon_{i,eff}$ are shown in Fig. 7. ε_s' and ε_i are also shown for comparison. Consideration of boiling point of Pd (2963°C) more then SiO_2 (2230°C), the actual weight-ratio of SiO_2 and Pd is larger than the prepared weight-ratio of SiO_2 to Pd after evaporation.

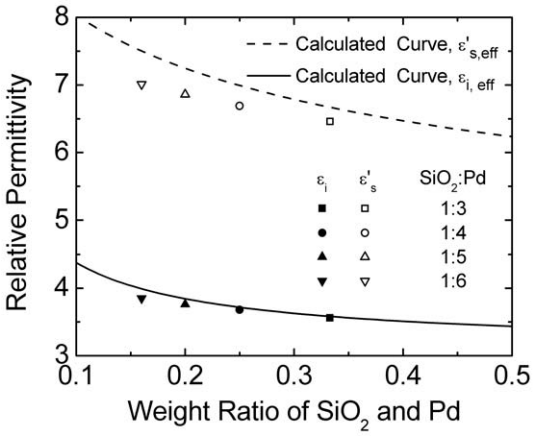

Figure 7. Calculated relative permittivity as a function of weight-ratio of SiO_2 and Pd. Fitting data for experimental I-V curve are included.
doi:10.1371/journal.pone.0050681.g007

Conclusions

In summary, characterization and modeling of MSM GaAs diodes using to evaporate SiO_2 and Pd simultaneously as the mixture electrode were investigated. Effects of operating at various temperatures and a mixture with the various weight-ratios of SiO_2 to Pd on electrical performances were investigated. ϕ_b and A* were determined to the thermionic emission process to describe well the current transport for Pd-MSM diodes in the consideration of the carrier over the metal-semiconductor barrier. In addition, in the consideration of the carrier over both the metal-semiconductor barrier and the insulator-semiconductor barrier simultaneously, thermionic emission process can be used to describe well the current transport for M-MSM diodes. Furthermore, in the higher applied voltage, the number of minority carriers at the semiconductor surface is larger then of the majority carrier. The carrier recombination will be taken into discussion. Besides, I_M was developed to evidence the concepts. Our calculated results are in good agreement with the experimental ones.

Author Contributions

Conceived and designed the experiments: SWT. Performed the experiments: SWT. Analyzed the data: SWT. Contributed reagents/materials/analysis tools: SWT SWL. Wrote the paper: SWT.

References

1. Tsai JH, Li CM, Liu WC, Guo DF, Chiu SY, et al. (2007) Integration of n- and p-channel InGaP/InGaAs doped-channel pseudomorphic HFETs. Electron. Lett. 43: 732–734.
2. Chen LY, Cheng SY, Chen TP, Chu KY, Tsai TH, et al. (2008) On an InGaP/InGaAs Double Channel Pseudomorphic High Electron Mobility Transistor with Graded Triple δ-Doped Sheets. IEEE Trans. Electron Devices 55: 3310–3313.
3. Hsu WC, Lee CS, Ho CS, Lai YN, Huang JC, et al. (2010) InAlAs/InGaAs MOS-MHEMTs by Using Ozone Water Oxidation Treatment. Electrochemical and Solid State Letters 13: H234–H236.
4. Lee CS, Chou BY, Yang SH, Hsu WC, Wu CL, et al. (2011) Investigations of Novel Γ-Gate MOS-HEMTs by Ozone Water Oxidation and Shifted Exposure Techniques. IEEE Trans. Electron Devices 58: 2981–2989.
5. Kang WP, Gurbuz Y (1994) Comparison and analysis of Pd- and Pt-GaAs Schottky diodes for hydrogen detection. J. Appl. Phys. 75: 8175–8181.
6. Schalwig J, Muller G, Karrer U, Eickhoff M, Ambacher O, et al. (2002) Hydrogen response mechanism of Pt–GaN Schottky diodes. Appl. Phys. Lett. 80: 1222–1224.
7. Lin KW, Chen HI, Chuang HM, Chen CY, Lu CT, et al. (2004) Characteristics of Pd/InGaP Schottky diodes hydrogen sensors. IEEE Sensors J. 4: 72–79.
8. Hung CW, Lin HL, Chen HI, Tsai YY, Lai PH, et al. (2006) A novel Pt/$In_{0.52}Al_{0.48}As$ Schottky diode-type hydrogen sensor. IEEE Electron Device Lett. 27: 951–953.
9. Huang JR, Hsu WC, Chen YJ, Wang TB, Lin KW, et al. (2006) Comparison of hydrogen sensing characteristics for Pd/GaN and Pd/$Al_{0.3}Ga_{0.7}$ as Schottky diodes. Sens. Actuators B, Chem. 117: 151–158.
10. Ali M, Cimalla V, Lebedev V, Tilak V, Sandvik PM, et al. (2006) A study of hydrogen sensing performance of Pt–GaN Schottky diodes. IEEE Sensors J. 6: 1115–1119.
11. Huang JR, Hsu WC, Chen HI, Liu WC (2007) Comparative study of hydrogen sensing characteristics of a Pd/GaN Schottky diode in air and N_2 atmospheres. Sens. Actuators B, Chem.123: 1040–1048.

12. Song J, Lu W (2008) Thermodynamic and kinetic analysis of hydrogen sensing in Pt/AlGaN/GaN Schottky diodes at high temperatures. IEEE Sensors J. 8: 903–909.
13. Tsai TH, Chen HI, Lin KW, Hung CW, Hsu CH, et al. (2008) Hydrogen sensing characteristics of a Pd/AlGaN/GaN Schottky diode. Appl. Phys. Express 1: 041102.
14. Lundström KI, Shivaraman MS, Svensson CM (1975) A hydrogensensitive Pd-gate MOS transistor. J. Appl. Phys. 46: 3876–3881.
15. Fogellberg J, Eriksson M, Dannetun H, Petersson LG (1995) Kinetic modeling of hydrogen adsorption/absorption in thin films on hydrogensensitive field-effect devices: Observation of large hydrogen-induced dipoles at the Pd-SiO2 interface. J. Appl. Phys. 78: 988–996.
16. Lu CT, Lin KW, Chen HI, Chuang HM, Chen CY, et al. (2003) A new Pd–oxide–$Al_{0.3}Ga_{0.7}As$ MOS hydrogen sensor. IEEE Electron Device Lett. 24: 390–392.
17. Filippov VI, Vasiliev AA, Moritz W, Szeponik J (2006) Roomtemperature hydrogen sensitivity of a MIS-structure based on the Pt/LaF3 interface. IEEE Sensors J. 6: 1250–1255.
18. Tsai YY, Cheng CC, Lai PH, Fu SI, Hong CW, et al. (2007) Comprehensive study of hydrogen sensing characteristics of Pd metal–oxide–semiconductor (MOS) transistors with $Al_{0.24}Ga_{0.76}As$ and $In_{0.49}Ga_{0.51}P$ Schottky contact layers. Sens. Actuators B, Chem. 120: 687–693.
19. Chiu SY, Huang HW, Huang TH, Liang KC, Liu KP, et al. (2008) High-sensitivity metal-semiconductor-metal hydrogen sensors with a mixture of Pd and SiO_2 forming three-deimnsional dipoles. IEEE Electron Device Lett. 29: 1328–1331.
20. Chiu SY, Huang HW, Liang KC, Huang TH, Liu KP, et al. (2009) GaN hydrogen sensor with Pd-SiO_2 mixture forming sensing nanoparticles. Electronic Lett. 45: 231–232.
21. Chiu SY, Liang KC, Huang TH, Liu KP, Huang HW, et al. (2009) GaN sensors with metal–oxide mixture for sensing hydrogen-containing gases of ultralow concentration. Jpn. J. Appl. Phys. 48: 041002.
22. Chiu SY, Tsai JH, Huang HW, Liang KC, Tsai TM, et al. (2009) Integrated Hydrogen-Sensing Amplifier With GaAs Schottky-Type Diode and InGaP–GaAs Heterojunction Bipolar Transistor. IEEE Electron Device Lett. 30: 898–900.
23. Sze SM, Ng KK (2007) Physics of semiconductor devices, 3rd ed. New York: John Wiley & Sons, Inc. 134–240
24. Rideout VL, Crowell CR (1970) Effects of image force and tunneling and current transport in metal-semiconductor (Schottky barrier) contacts. Solid-State Electron. 13: 993–1009.